Experimental and molecular dynamic insights on the thermophysical properties for MWCNT-Phosphonium based eutectic thermal media

Nipu Kumar Das [a], Papu Kumar Naik [a], Dhileep N. Reddy [b], Bhabani S. Mallik [b], Suryasarathi Bose [c], Tamal Banerjee [a],*

[a] Department of Chemical Engineering, Indian Institute of Technology Guwahati, Guwahati 781039, Assam, India
[b] Department of Chemistry, Indian Institute of Technology Hyderabad, Hyderabad 502284, Telangana, India
[c] Department of Materials Science and Engineering, Indian Institute of Science Bangalore, Bangalore 560012, Karnataka, India

ABSTRACT

In this study, a thermal media is synthesized by mixing hydrogen bond acceptor (HBA) [Methyltriphenylphosphonium bromide (MTPB)] salt with hydrogen bond donor (HBD) [ethylene glycol] at a molar ratio of 1:4. Thereafter the corresponding nanofluid was prepared by dispersing 0.02 wt% Multi-Walled Carbon Nanotube (MWCNT) having a diameter 10–30 nm in the base fluid. Prior to dispersion, the shape and morphology of the MWCNT were ascertained using both Field Emission Scanning Electron Microscope (FESEM) and Field Emission Transmission Electron Microscope (FETEM). The crystallinity and functional groups were investigated by X-ray Powder Diffraction meter (XRD) and Fourier Transform Infrared Spectroscopy (FTIR). The stability of the prepared nanofluid was initially performed using visual observation followed by zeta potential measurements. Thermogravimetric analysis (TGA) was performed to check the stability of nanofluid at a temperature close to 500 °C at a heating rate of 10 °C/min under nitrogen environment. Thermophysical properties such as density, viscosity, thermal conductivity, and specific heat of nanofluid were measured in the temperature range 25–85 °C. It is evident from the experimental data that viscosity and density decrease with an increase in temperature. On the contrary, the specific heat and thermal conductivity of the nanofluid were found to increase with temperature. This is due to the induced Brownian motion of the nanoparticle, which results in higher kinetic energy at high temperature. In the penultimate section, Molecular Dynamic (MD) simulations were performed to compare and validate the results of thermal conductivity of nanofluid.

© 2022 Elsevier B.V. All rights reserved.

1. Introduction

Environmental concerns have initiated researchers to create alternative, inexpensive, efficient, and sustainable energy sources due to the global warming induced by fossil fuel use. In terms of environmental concerns, the green solvent is one of the alternate methods for reducing the impact of pollution in applications such as extraction and thermal media. The use of green solvent or technology reduces wastewater pollutants, toxic chemical substances and also improves technology. Here 'green' refers to the preparation of chemicals such as solvents and fluids through non-fossil fuel sources. Pharmaceutical companies are now using greener synthesis routes for drug development so as to reduce pollution and manufacturing costs [1].

Deep Eutectic Solvents (DES) are a new class of organic solvents. It is gaining attraction due to its various beneficial physical and chemical properties [2–5]. They are analogous to Ionic Liquids (IL's), which are known for recent industrial applications[6]. Applications concerning IL's for extractions are also well documented [7–10]. The physicochemical properties of ILs are similar to DES and include low volatility, low flammability, higher thermal and chemical stability. For their interesting properties, IL's are alternative to conventional organic solvents [11–13]. But due to its high manufacturing and toxicity issues, primarily from their petroleum-based precursors, alternative solvents are still gaining importance. Further, most of the IL's are highly viscous and difficult to synthesize. With respect to thermal media, Wu et al. [14] synthesized IL's namely [C$_4$min] [PF$_6$], [C$_8$min] [PF$_6$], and [C$_4$ min] [Tf$_2$N] (Tf$_2$N: bis trifluoromethane sulflonimide) and used them as heat transfer fluid for solar thermal power plant.

Ionic liquids (ILs) can also be referred to as green solvents due to their excellent thermal and chemical stability and low volatility.

But, they are less desirable in nanofluid applications due to their high toxicity and non-biodegradability as the most of them has precursors based on petroleum. Further the complicated procedure of preparing ILs hinders it application as unlike DES, it requires a number of unit operations for its synthesis. Compared to IL, DES-based nanofluids are more environmentally benign and scale-up-friendly as some of them originate from natural precursors (betaine, urea) and are known as Natural Deep Eutectic Solvents (NADES) [15]. As the base fluid is formed by combining HBA and HBD, no waste product is generated throughout the preparation. This is why the current DES is adopted as base solvent in heat transfer applications due to their low viscosity and density. Industrially, DES-based nanofluids offer a more significant potential for usage as heat transfer fluids and energy harvesting applications than IL-based nanofluids [16].

Due to its attractive beneficial and enhanced properties, DES has promised several industrial applications in the food processing, power, extraction, and nanotechnology domains. Generically, DES are formed by mixing defined amount of Hydrogen Bond Donor (HBD) and Hydrogen Bond Acceptor (HBA). These are a certain class of liquids at ambient conditions (freezing points below 25 °C), which are binary compositions of two components, a Hydrogen Bond Donor(HBD) and a Hydrogen Bond Acceptor (HBA), each of which has a melting point above that of the DES; hence they are eutectics. According to Abott et al. [4] the lattice energy decides the interaction between HBD and HBA and also point out the formation of an eutectic mixture. DES are subgroup of room-temperature ionic liquids (RTILs) but are binary mixtures contrary to ordinary IL's that are single substances. It has been said that DES are not novel compounds or a new type of compound but binary or ternary mixtures. Further, the presence of a eutectic point in a mixture cannot be used to define or characterize a DES since essentially all mixtures of compounds immiscible in the solid phase will present a eutectic point. Chen and Mu [17] used DES to treat and dissolve chemicals from biomass. Shisov et al. [18] reported various applications of DES in analytical chemistry. They also used DES to improve the nanoparticle extraction efficiency and used it in chromatography as a mobile phase additive.

Choi et al. [19] first introduced the term 'nanofluid', which defines as a liquid containing nanometre size particles. Nanofluid is employed as an excellent heat transfer medium in many practical applications due to its enhanced physical features [20–22], such as density, dynamic viscosity, specific heat, and thermal capacity. Several studies have been conducted using dispersed nanoparticles to assure the enhancement of the nanofluid's physical properties and thermal stability. Carbon nanotubes (CNTs) have sparked a lot of attention in recent years due to their exceptional electrical and mechanical capabilities [23]. Multi-walled carbon nanotube containing nanofluid leads to the enhancement of thermal conductivity. The increase of the ultra-sonication time is also known to increase the fluid's thermal conductivity up to a certain extent [24]. Similar work has been reported by Mahbubul et al.[25] where they studied the effect of ultra-sonication time on the stability and rheological properties of the nanofluid containing 0.5 vol% of spherical Al_2O_3 nanoparticles. They reported that increasing the ultra-sonication period leads to a decrease in the NF's dynamic viscosity. Y. Hwang et al. [26] used various nanoparticles such as MWCNT, fullerene, CuO, SiO_2 to prepare nanofluid in (a)water, (b) ethylene glycol, and (c) oil as a working fluid. The experimental results show that the thermal conductivity of the nanofluid rises as the volume fraction increases except for water-based fullerene nanoparticles.

Borode et al.[27] reported application of carbon nanotube-based nanofluid in the heat exchanger. The result shows that carbon-based nanofluid can improve the performance of the heat exchanger and reduce the heat exchange area. Ilyas et al. [28] synthesized Multi-walled carbon nanotube(MWCNT) and observed the stability of thermal oil-MWCNT based nanofluid at various concentrations 0–1 wt%. Similar work has been done by Salam and Burk [29], where they studied functionalized MWCNT with Poly-ethylene Glycol (PEG) and octadecylamine (ODA). Carbon-based nanoparticles can be used in industrial cooling operations [30], automotive cooling applications [31], electronic cooling (microchip cooling)[32,33], extraction of geothermal power and other energy sources [34], microscale fluidic applications [35] and solar desalination system [36]. All the application has been benefited from the use of using DES as a base fluid in the preparation of nanofluids. Nanofluids based on DES, may be also used in biomedical applications such as nanodrug delivery [37,38], nanocryosurgery [39] and cancer therapies [40] due to their low toxicity and environmental friendliness. Due to its high thermal conductivity, DES/MWCNT nanofluid is particularly well suited for heat transfer applications. The DES/MWCNT-based nanofluid has the potential to be used in multistage flash solar desalination systems.

In this current work (MTPB) as HBA and EG as HBD were mixed in the molar ratio 1:4 and used as base fluid. After that, the nanofluid with MWCNT were prepared using a two-step method, by dispersing 0.02 wt% nanoparticles. Thermophysical properties of the MTPB-EG based DES and the thermal stability of the nanofluid were thereafter analyzed at high temperatures. In the penultimate section, the thermal conductivity was compared and validated with the results obtained from the Non Equilibrium Molecular Dynamics simulations.

2. Experimental details

2.1. Materials

Ethylene glycol (EG)(C$_2$H$_6$O$_2$) with > 99% purity was obtained from Merck India. Methyltriphenylphosphonium bromide (MTPB) (C$_{19}$H$_{18}$BrP) was purchased from SRL India Pvt. Ltd. with > 98% purity. Multi-Walled Carbon Nanotube (MWCNT) with 10–30 nm diameter and 5–15 μm length was obtained from TCI chemicals. The composition of DES was confirmed by Nuclear Magnetic Resonance Spectroscopy (^{1}H NMR). The chemical composition of MTPB, EG, and optimized structure of MWCNT are shown in Table 1 and Fig. 1.
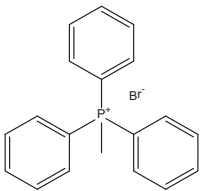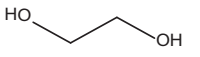
### 2.2. Characterization of Multi-Walled carbon nanotube (MWCNT)

The morphology and shape of MWCNT nanoparticles were investigated by Field Emission Transmission Electron Microscope (FETEM, JEOL-JEM2010) and Field Emission Scanning Electron Microscope (FESEM Sigma 300, Zeiss). The crystallinity structure of MWCNT was analyzed by Powder X-ray Diffraction (XRD Bruke D8, advanced X-ray diffraction measurement system) at room temperature in the range of 2θ from 10 to 80°. Fourier Transform Infrared Spectra analyzer (FTIR, Perkin–Elmer, Norwalk, USA) was used to ascertain if any functional groups or chemicals were present in MWCNT and the nanofluid. The absorption spectra were recorded in the range between 500 and 4000 cm^{-1}.

2.3. Synthesis of DES

In this work, DES was prepared by mixing 1 mol of MTPB and 4 mol of Ethylene Glycol in a round bottom flask. A reflux condenser was used to minimize the loss of vaporization. The mixer was stirred continuously on a magnetic stirrer hot plate (TARSONS SPINOT magnetic stirrer/hot plate-DIGITAL, MC 02, India) for 24 h until a clear liquid was formed. The mixer was kept overnight at room temperature to observe solidification. When two compo-

Table 1
Chemical compositions of DES.

Name	CAS No.	Chemical Structure	Molecular formula	Number of moles
Methyltriphenylphosphonium bromide [MTPB]	1779–49-3		$C_{19}H_{18}BrP$	1
Ethylene glycol [EG]	107–21-1		$C_2H_6O_2$	4
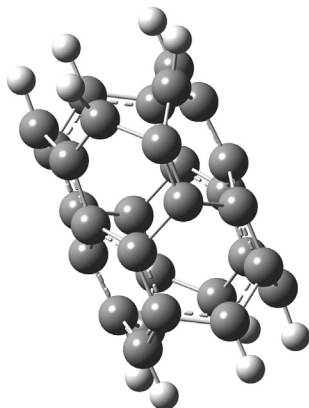
Fig. 1. Representative structure of carbon nanotube.

nents with higher melting points are mixed in a defined molar ratio, the resulting melting point is called eutectic point, which is less than the melting point of the individual component. DES are not novel compound or a new type of compound, but binary or ternary mixtures. It should be noted that the presence of a eutectic point in a mixture cannot be used to define or characterize a DES since essentially all mixtures of compounds immiscible in the solid phase will present a eutectic point Abott, et al. [4] attributed the first DES to a choline chloride and urea combination in 2003. Choline chloride has a melting point of 302 °C, while urea has a melting point of 133 °C. Their combined melting point is 120 °C, which is lower than the melting points of urea and ChCl. The molar ratio can also be predicted by the COSMO-SAC model [17], where solid Liquid Equilibria (SLE) prediction can be made prior to experimentation. In our work, we refer the DES or eutectic mixture to the pair HBD-HBA with a eutectic point dependent of the specific composition we are working with. From analysis of the ^1H NMR spectra of the prepared DES, we can confirm the (4:1) molar ratio of the DES.

2.4. Preparation of nanofluids

The nanofluid formation is the vital step that shall help us enhance the thermal characteristics of heat transfer fluid. The agglomeration of the solid particle is critical and if it occurs, it shall lead to poor thermophysical properties of DES-based nanofluid. Agglomeration, cluster formation, and faster settlement in fluids are usually caused by high surface energies and subsequent interactions of nanoparticles. To maintain the improved thermal characteristics, a stable nanofluid must be synthesized. The maximum stability time can be defined as the amount of time that the nanofluids remains completely scattered [41].

Overall there are two primary methods for preparing nanofluid [42–45], namely: two-step method and one-step method. However, both methods have some advantages and disadvantages. Within the two-step preparation method, the first stage consists

of the synthesis of nanotubes or nanofibres, in the form of dry powders via physical or chemical methods. Thereafter the synthesized dry powders are dispersed in base fluids. This process is recommended for the production of large-scale nanofluids [46,47]. The size and shape of the nanoparticles are easily controlled in a two-step method. To alleviate the possible settling of the nanofluid, ultrasonication and mechanical stirring are used to improve nanofluid dispersion. In the single-step process, the nanoparticle and base fluid are prepared and simultaneously dispersed to form nanofluid [42,48]. Although the one-step method gives good stability and dispersion of the nanofluid, there is complexity involved in the preparation method where the size, shape and concentration of the nanoparticles are difficult to control. Hence, we have adopted the two step process where the nanoparticle was directly purchased.

In this work, the dispersion stability of nanofluids are checked by performing Zeta potential measurement through Delsa Nano (Delsa Nano C, BECKMAN COULTER). A thermogravimetric analyzer (TGA) is used to determine the thermal stability of the nanofluid. The nanofluid is prepared by mixing 0.02 wt% of MWCNT in DES. Initially, the mixture of solvents and MWCNT were mixed on a vortex mixer (SPINX MC-01, Tarsons). After mixing, the mixture was placed in an ultra-sonication chamber (GT-1990QTS) to get a homogeneous and uniform suspension of particles which prevented the agglomeration of carbon nanotube.

2.5. Thermophysical properties

Measurement of thermophysical data of nanofluid gives information about the transport system of the fluid. The nanofluid was characterized by thermo-physical properties like density, viscosity, thermal conductivity, and specific heat capacity. All these properties were measured at different temperature ranges. The densities of DES and DES + MWCNT nanofluids were measured by using an Anton Paar Densitometer (DMA 4500 M) at various temperatures ranging from 25 to 85 °C. The accuracy of density measurement was estimated as 0.0001 g/cm³. Density is the critical parameter for calculating the pressure loss and pumping power, and it works on the basis of the U-tube Oscillatory concept. It is made out of a single U-shaped glass tube that is stimulated and oscillates at a particular frequency. That frequency calculates the density of the sample.

Rheological properties of the nanofluid were measured using Anton Paar Interfacial Rheometer (Phsica MCR301). Viscosities were calculated within the temperature range 25–85 °C with an accuracy of ± 5%. The shear rate was measured in the range of 0–85 s⁻¹. The rheometer consists of a round parallel plate that is used to measure viscosity at various temperature ranges. The thermal conductivity of DES and nanofluids was measured by KD2 pro thermal analyzer (Decagon Device, USA) at different temperatures with an accuracy of ± 0.0096 W/m K. KD2 pro thermal analyzer

worked on the principle-based on hot wire method. Specific heat capacity was measured by performing Temperature Module Differential Scanning Calorimeter (TMDSC: NETZSCH STA 449F3) at a temperature from 45 to 90 °C. Sapphire is used as standard comparison material under nitrogen environment at a heating rate of 10 °C/min. It was based on the principle of heat flow, which is a function of temperature that maintains sample and reference at the same temperature.

2.6. Stability analysis

The particle–particle intermolecular force van der Waals attraction force dominates the other repulsive forces as it causes rapid settlement and agglomeration between the particles [46,49]. As a result, it increases the size of the clusters, which may cause the reduction in thermal properties of the nanofluid. Therefore, the stability analysis of nanofluid is important before its use in application such as direct solar thermal absorption. We have adopted both visual observation and zeta potential analysis for the stability of the nanoparticles.

2.6.1. Visual observation and optical microscopy

Here the nanofluid was prepared by a two-step method and sonicated for 8–10 min to make the suspension homogenous. The prepared nanofluid was kept at room temperature for four weeks undisturbed. Visual observation was formulated to view the settling of the nanofluid. Cluster size and nanotube dispersion in the nanofluid were observed by capturing the images through an optical microscope (Axiostar plus, Carl Zeiss, Germany). The microscopic images were thereafter analyzed to study the particle dispersion in the working fluid.

2.6.2. Zeta potential measurement and thermo Gravimetric analysis (TGA)

Zeta potential measurement was measured by Delsa Nano (Delsa Nano C, BECKMAN COULTER) instrument to see the stability and particle size distributions of the particles in nanofluid. The electrical potential created at the solid–liquid interface as a result of the relative mobility of solid particles and liquid is referred to as the zeta potential [50]. According to Mehrali et al [51], the zeta potential value of − 30 mV to + 30 mV is considered stable. Whereas, Vandsburger [52] considered moderate stability when the zeta potential value is close to ± 30 mV. A value close to 45 mV ensures the complete stability of nanofluids. The high stability of the nanofluid system is demonstrated by a zeta potential value greater than ± 60 mV [53]. Thermo Gravimetric Analysis (TGA) (TG209 F1, Libra, NETZSCH, Germany) was also performed to determine the thermal stability of the nanofluid. The sample was studied under nitrogen atmosphere at a heating rate of 10 °C/min.

3. Computational details

Classical molecular dynamics (MD) simulations were performed with the use of GROMACS 5.0.4[54,55] and LAMMPS [56] software. The equilibration was carried out with GROMACS 5.0.4, and thermal conductivity calculations were performed with LAMMPS. OPLS-AA force fields were used to define the bonded and nonbonded terms[57]. The charge scaling of 0.8 was applied to the HBA and HBD similar to Ionic Liquids[58]. This is analogous in comparing the charge transfer effect in ILs. Earlier work has reported a scaling factor of 0.9 on the ions of [C₄mim][Cl] to give better results[59]. We have also showed that charge scaling factor gives appropriate structure and physical properties in one of our earlier studies[60].
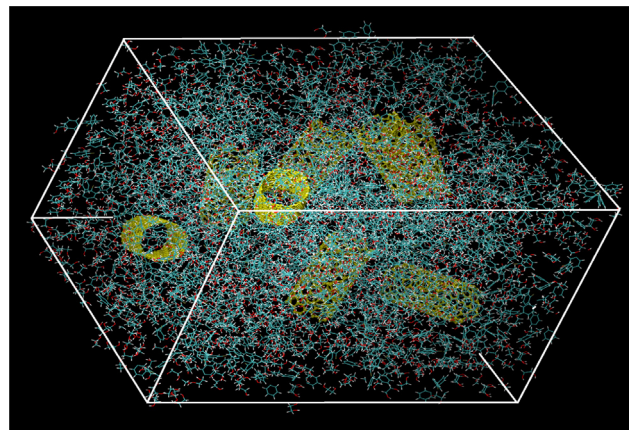

Fig. 2. MD snapshot of the system.

The initial structure of carbon nanotubes (CNT) was generated using the VMD software [61]. The *g_x2top* tool from the GROMACS 5.0.4 was used to generate the force field for the CNT. The HBA and HBD were optimized using Gaussian software[62] with B3LYP[[63–65] method and 6–311 + G(2d,p) basis set. Partial charges were generated using the Antechamber package[66]. For the overall periodic box,8 carbon nanotubes, 1600 ethylene glycol (EG) molecules, and 400 HBA (Methyltriphenylphosphonium bromide, MTPB) and 100 HBD (ethylene glycol)were randomly packed into the cubic cell using Packmol software[67] (Fig. 2).

Generated structure from the Packmol software were then used for further simulations in GROMACS. Energy minimization was performed using the steepest descent method[68]. After energy minimization, the system is heated above 200 K when compared to the target temperature in the NVT ensemble. Thereafter the system was cooled to the respective temperature using the annealing method. In the annealing procedure, the temperature is decreased by 20 K for each nanosecond run for 10 steps. Surface effects were eliminated using the periodic boundary conditions. Integration of the equations of motion was carried out using Velocity-Verlet algorithm. Bonds that are linked to hydrogen atoms were constrained using the LINCS algorithm. 10 ns equilibration was carried out using the NVT ensemble at the target temperature. 10 ns *NPT* run was performed using the V-rescale thermostat[69], using the Berendson barostat [70], with coupling constants of 0.1 and 2.0 ps, respectively. A 20 ns run in NPT run was performed using V-rescale thermostat [69] and Parrinello-Rahman[71] barostat. The V-rescale thermostat was used in the NVT ensemble for 20 ns. GRO2LAM software was used to convert the topology from GROMACS format to LAMMPS. 20 ns simulation was done to calculate the thermal conductivity. The reverse non equilibrium molecular dynamics (RNEMD) procedure was used to evaluate the thermal conductivity [72]. RNEMD is a widely used technique in previous literature [73–76]. Time step of 2 fs was used throughout the simulations. Cut off for nonbonded interactions was 1.2 nm.

4. Results and discussions

4.1. ¹H NMR of DES

The composition of the DES was confirmed by ¹H NMR (Fig. 3). The absence of extra peaks in the spectra implies that there is no chemical reaction, and the mixture is stable. The details of ¹H NMR analysis have been reported in our previous publication [77].
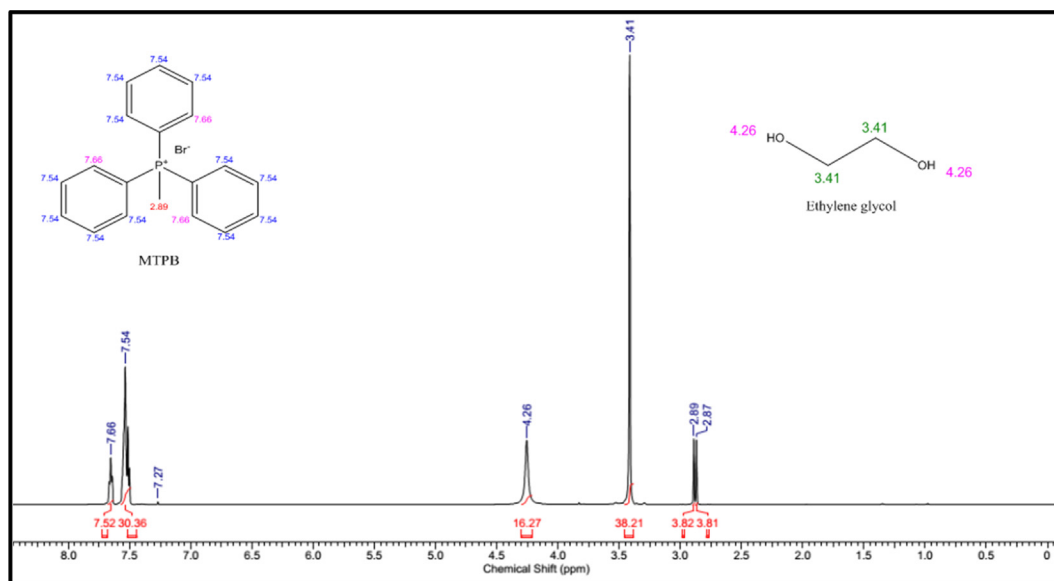
Fig. 3. NMR spectra of pure DES ^{1}H NMR.

4.2. Characterization and morphological studies

Field Emission Transmission Electron Microscope (FETEM) was used to investigate the shape and morphology of the MWCNT nanoparticle. Fig. 4(a) & (b) and 4(c)&(d) shows the FETEM and FESEM images of MWCNT with 200 nm and 100 nm scales, indicating that the diameter varies from 30 nm to 50 nm. This diameter was confirmed by Scanning Electron Microscope (SEM) with 200 nm and 100 nm scale. Fig. 5(a) shows the X-ray diffraction pattern of multi-walled carbon nanotube (MWCNT). A sharp peak at (0 0 2) plane $2\theta = 26.4°$ is visible. This implies the periodicity of the atom in MWCNT. However, low-intensity peak at (1 0 0), (0 0 4) and (1 1 0) planes at $2\theta = 43.04°$, $2\theta = 53.68°$, $2\theta = 78.0°$ clearly indicates the crystalline structure of the MWCNT. No other peaks were observed, which implies the high purity and non-functionality of the nanotube. Fourier transform infrared spectroscopy (FT-IR) analysis of MWCNT, and DES-based nanofluid is shown in Fig. 5(b). Characterization of FTIR spectroscopy was performed to analyze the presence of functional groups or impurity on the multi-walled carbon nanotube (MWCNT). Different peaks were observed in the medium infrared region where wave number ranges between 500 and 4000 cm^{-1}. An absence of a peak in FTIR MWCNT spectra negates the presence of functional groups, impurities, or C = C attachment. Further, there is no hydroxyl group (–OH) group as the analysis was performed in a moisture-free environment.

4.3. Stability analysis

4.3.1. Visual observation and optical microscopy

In the initial part, visual observation was used to analyze the stability of the nanofluid. Photographs of nanofluid were taken after sonication within a gap of 15, 20, and 29 days respectively, as shown in Fig. 6(a). On visual inspection, there is no precipitation observed initially for the first two weeks. However, slight precipitation was observed on the 20th day, and some particles were observed to settle on the 29th day (Fig. 6(a)). The visual observation method from the figure shows that 0.02 wt% MWCNT based nanofluid gave excellent stability till 15–20 days.

Fig. 6(b) depicts optical microscopic pictures that reveal the homogeneous dispersion of nanoparticles in the working fluid.

The photograph was captured in a high-resolution magnitude of 10X and 20X. From the images, it was noticed that nanoparticles are uniformly distributed in the DES base fluid. Images were captured by a normal light microscope, so it could not determine the accurate size and shape of the nanoparticle. However, it can provide a quality evaluation of the size of the nanoparticle in the base fluid.

4.3.2. Zeta potential and thermo Gravimetric analysis (TGA)

Thermo Gravimetric Analysis (TGA) was performed to determine the thermal stability of the nanofluid. TGA was performed at a heating rate of 10 °C/min under nitrogen atmosphere. The degradation of MWCNT-DES nanofluid with respect to the temperature is shown in Fig. 7. Two-stage mass losses were observed in the phosphonium-MWCNT based nanofluid. Degradation of the nanofluid was first observed at 96.88 °C when the sample was heated from 25 °C to 500 °C. Thereafter degradation was observed from 110 °C, which ends at ∼ 180 °C. The second weight loss was observed at 328.22 °C. Complete decomposition was observed at 400 °C. Thereafter, a gradual loss was observed when heated up to 500 °C. In TGA, the two-stage degradation of the nanofluid indicated the high thermal stability of the nanofluid till 320 °C.

The isothermal TGA has been done under nitrogen atmosphere at the heating rate of 20 °C/min for 12 h. DES based nanofluid shows rapid degradation after heating the samples at 80 °C, 120 °C and 160 °C respectively (Fig. 8). The thermal stability of the fluid is around the order of 50–60 min. It is visible from Fig. 8 that the mass loss is very high at the beginning of the heating process primarily at higher temperatures of 120 °C and 160 °C and then almost constant after 100 min. Around 35% and 39% mass loss was observed at temperatures 160 °C and 120 °C respectively, whereas approximately 22% mass loss was observed at temperature 80 °C. The steady outcome can be attributed to the low weight concentration of the nanoparticle in the deep eutectic solvent [78,79].

Zeta potential measurement were performed to check the dispersion and stability of the nanofluid through the observation of electrokinetic potential [80,81]. From definition, two seperate layers arise around nanoparticles when they are distributed in the base fluid. The stern layer is the layer that is connected to the particle. The diffuse layer, the layer below the stern layer, is weakly
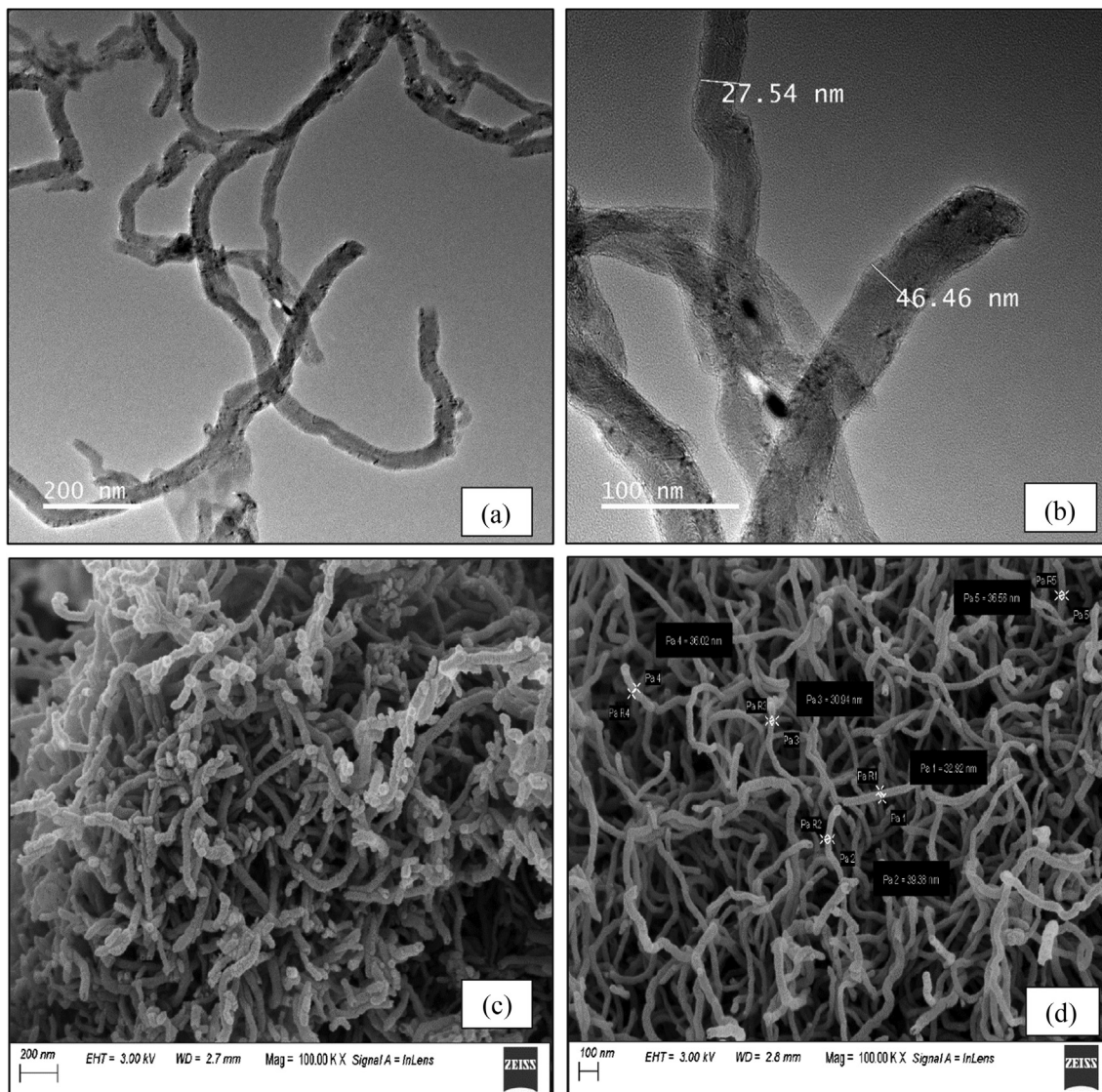
Fig. 4. Field Emission Transmission Electron Microscope (FETEM) with scale (a) 200 nm; and (b) 100 nm and Field Emission Scanning Electron Microscope (FESEM) images of MWCNT with (c) 200 nm and (d) 100 nm.

bonded by the nanoparticle. The combination of both layers is electrically neutral and hence is known as the electric double layer (EDL). Zeta potential is generated in the interface of EDL and here is measured in millivolts (mV). A high zeta potential indicates stronger repulsive forces, which increases the probability of particle agglomeration. The nanoparticle's large surface area and small size combines to reduce their surface area, resulting in strong van der Waal forces. The strong van der Waal forces attract the other particles, resulting in the formation of an agglomeration. According to Vandsburger [52], nanofluids are nearly stable when particles having a zeta potential value is near about ± 30 mV. If the zeta potential value is close to 45 mV, the stability of nanofluids is ensured. Nanofluid gives excellent stability if its value lies above ± 60 mV. Fig. 9 represents the value of the zeta potential curve, which came to be −90.12 mV indicating high stability.

4.4. Density and viscosity

Density is an essential factor for heat transfer fluid as it determines the flow behavior of the fluid. Experimentally measurement of density is reported in Fig. 10(a) and compared with commer-cially available heat transfer fluid Therminol VP-3 (Phenylcyclohexane + bicyclohexyl) [82]. The experimental data indicated that the density of both DES and nanofluid decreases with temperature from 25 to 85 °C. Also, it was noted from the fig-ure that the density of both nanofluid and DES is more than that of commercial fluid Therminol VP-3. Experimentally, nanofluid con-taining 0.02 wt% of MWCNT has low density than that of the base fluid. However, measured density variation between the DES and nanofluid is insignificant. This is attributed to the size of the nanoparticle. Here, thermal expansion occurs due to the increase in temperature, which results in higher kinetic energy of the mole-cules. A linear correlation was established between density and temperature as provided in equation (1) with regression value R^2 = 0.99952 and standard error value.$\pm 4.542 \times 10^{-6}$

$$\rho = 1.2417 - 7.16 \times 10^{-4}T \pm 4.542 \times 10^{-6} \qquad (1)$$

Where $\rho(\text{gm/cm}^3)$ is the density and T (K) is the temperature of the DES or Nanofluid.

Experimentally measured values are compared with the avail-able conventional mode namely Pak and Cho model [83], given
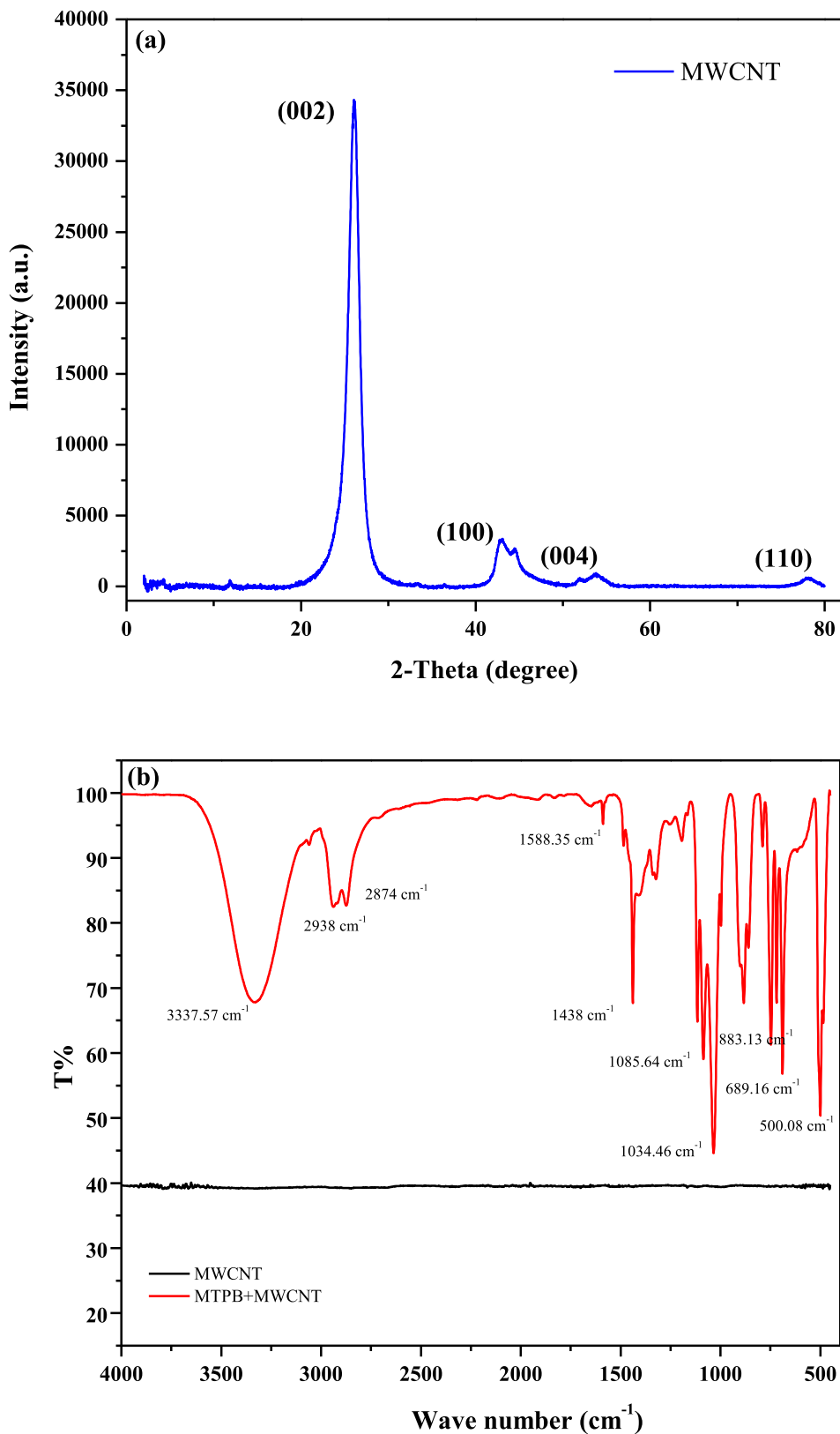
Fig. 5. (a) XRD pattern of MWCNT (b) FTIR spectra of MWCNT and nanofluid.

in equation (2). This model is based on the volumetric concentration and pure density of nanoparticle and base fluid. To compare the experimental results to this model, we have used equation (3) to convert the weight fraction into volume fraction.

$$\rho_{nf} = \varphi_v \rho_{np} + (1 - \varphi_v) \rho_{bf} \tag{2}$$

Where, ρ_{nf}, ρ_{np}, ρ_{bf} and φ_v are the density of nanofluid, nanoparticle, base fluid, and volume fraction of nanoparticle, respectively.
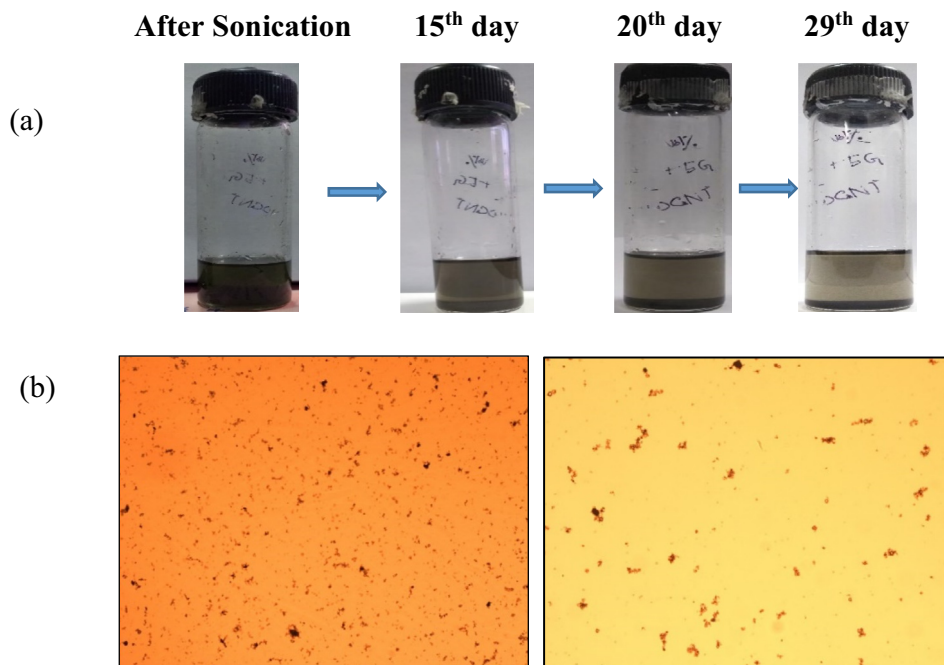
Fig. 6. (a) Digital Photos and (b) Optical microscopic images of nanofluid with high resolutions, 10x and 20x.
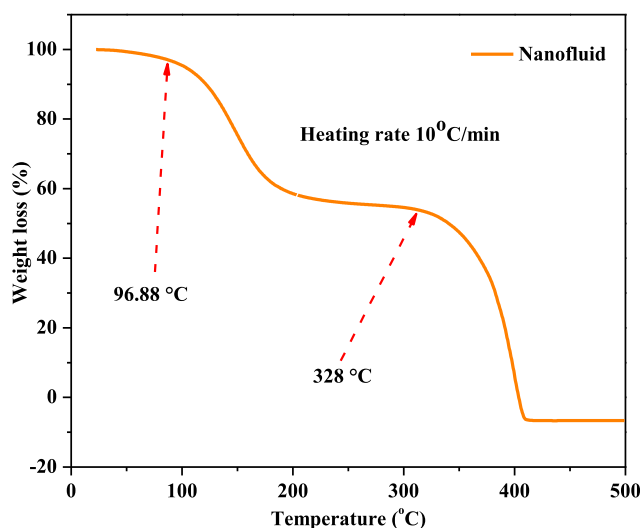

Fig. 7. TGA Analysis of MTPB based nanofluid (Heating rate 10 °C/min at nitrogen atmosphere).

Fig. 8. Isothermal TGA of DES + MWCNT nanofluid at different temperatures.

$$\varphi = \left[\frac{\left(\frac{m}{\rho}\right)_{Nanoparticles}}{\left(\frac{m}{\rho}\right)_{Nanoparticles} + \left(\frac{m}{\rho}\right)_{basefluid}} \right] \times 100 \qquad (3)$$

Where φ, m, and ρ denote volume fraction of the nanoparticles (%), solid mass (kg), and density (kg/m^3) of the nanoparticle, respectively. It was seen from the Fig. 10(b) that the results of the Pak and Cho model were very close to the experimental data.

Experimental measurement of viscosity for both DES and nanofluid were performed at different temperatures for a constant shear rate ($d\gamma/dt = 50\ sec^{-1}$) (Fig. 11(a)). It is observed that the viscosity of DES decreases with an increase in temperature from 25 to 85 °C. Similar results are observed when 0.02 wt% of MWCNT is added into the DES. Here the viscosity of the nanofluid decreases from
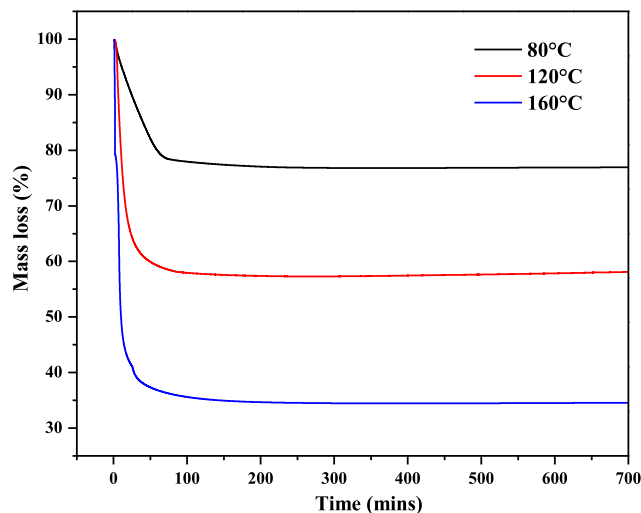
89.1 cP to 9.9 cP when temperature increases from 25 to 85 °C. Both the nanofluid and DES show higher viscosity than commercial fluid *Therminol VP-3*. However, it was observed that the presence of DES makes the inherent viscosity lower than the base fluid. It was also observed that the viscosity decreases exponentially with temperature. An exponential correlation was established with a regression value of $R^2 = 0.99$ to predict the viscosity of the different volume concentrations of the nanofluid.

$$\mu = 0.00684 + 0.3523e^{-0.05947T} \qquad (4)$$

Here μ is the viscosity in Pa.s and T is the temperature of the nanofluid in Celsius. It should be noted that a lower viscosity of the nanofluid results in lower pressure drop, which lessens the pumping costs. The measured experimental viscosity values were compared with the available theoretical model; Brinkman model [84] as given in equation (5).
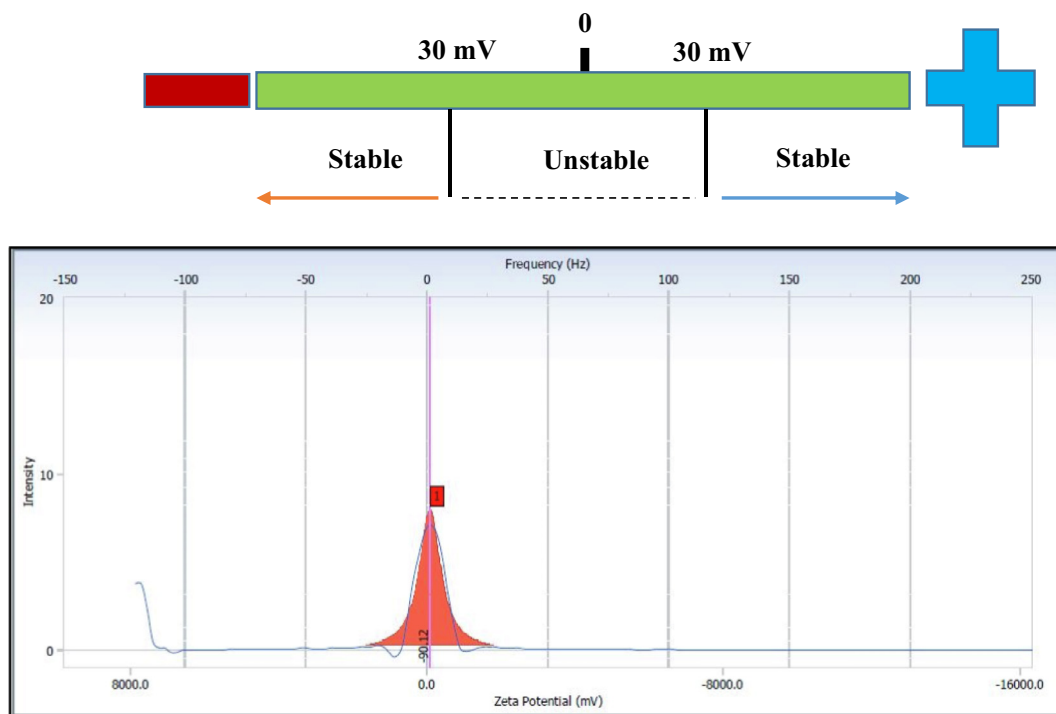
Fig. 9. Zeta potential results of [MTBP][EG] + MWCNT.

$$\mu_{nf} = \frac{\mu_{bf}}{(1 - \varphi)^{2.5}} \tag{5}$$

Where, μ_{nf} and μ_{bf} are the viscosity of nanofluid and base fluid, respectively. φ is the volume fraction. It should be noted that the Brinkman model (Fig. 11(b)) is suitable for bigger nanoparticle size, therefore the results for viscosity in smaller nanoparticle size is not accurate. Furthermore, the effect of temperature is not considered in this model. Newtonian fluid behavior of the nanofluid was confirmed from shear stress and shear rate data. From Fig. 12, a linear trend was observed at three different temperatures, namely 25 °C, 30 °C, and 35 °C. The data were obtained from different shearing times indicating the fluid's Newtonian behavior. Fig. 12 shows that as expected viscosity is strongly dependent on temperature.

We compared the obtained thermo physical properties with literature and observed the same results as Ilyas et al. [28,85], who reported a minor difference in density between base fluid and nanofluids which is consistent with our findings. According to published data, the density difference between MWCNT-thermal oil nanofluid and base fluid was 0.76 kg/m³ and 0.61 kg/m³ at 30 °C and 40 °C, respectively. Our investigation found that the density changes between 30 °C and 40 °C were 0.001 and 0.002 kg/m³, respectively. Similarly, the viscosity of the reported nanofluid and base fluid decreases with increased temperature, consistent with the literature [28]. Beheshti et al. [86] reported a 0.9% decrement of viscosity in nanofluid (MWCNT + Transformer oil) with 0.01 wt% concentration. This work reported, 11.3% and 9.5% decrement at 30 °C and 40 °C in 0.02 wt% DES-based nanofluid. However, the literature showed the opposite result [28], where 11.8% and 11.3% increments were found in 0.1 wt% nanofluids at 30 °C and 40 °C respectively.

4.5. Thermal conductivity and specific heat

Thermal conductivity of both base fluid and nanofluid were measured against different temperatures and shown in Fig. 13(a). The thermal conductivity of DES and nanofluid was first measured from 25 to 80 °C. It was noted that the thermal conductivity of nanofluid gradually increases with temperature. However, the thermal conductivity of DES decreases with an increase in temperature from 25 to 80 °C. From the experimental data, it was evident that the addition of MWCNT in the base fluid enhances the thermal conductivity as compared to the base fluid and commercial fluid *Therminol VP-3*. The enhancement of thermal conductivity was calculated from equation (6) [28].

$$TCE = \left(\frac{k_{nf}}{k_{bf}} - 1 \right) \times 100\% \tag{6}$$

The maximum enhancement of thermal conductivity was found at 361%. This is due to the interaction between the nanoparticles and the induced Brownian motion of the nanoparticle at high-temperature as nanoparticles can gain higher energy which increases their kinetic energy and leads in efficient transfer of heat. Nanoparticle's size and shape are another important factor which influence the thermal conductivity. Dong and Chen [87] reported the nanofluid thermal conductivity increases as the particle size decreased. In case of carbon nanotube nanoparticle, thermal conductivity increases with increase in the orders of large volume to surface ratio. Similar analogy was followed by Jhang and Choi [88] where it was observed that the thermal conductivity increases with the increase in size of the carbon nanotube. An exponential correlation of thermal conductivity as a function of temperature was developed for nanofluid with a regression value $R^2 = 0.91993$, as shown in Fig. 13(a).

$$\kappa = 0.19607 + 4.3669 \times 10^{-5} e^{(0.09218T)} \tag{7}$$

Here, κ and T are the thermal conductivity in W/mK and Temperature in Kelvin respectively. Molecular diffusion takes place in DES at increased temperature and it becomes faster when temperature gradually increases. Because, DES molecules are closely packed, heat transfer occurs through conduction mode. Due to increase in temperature, it allows the liquid to expand. The free
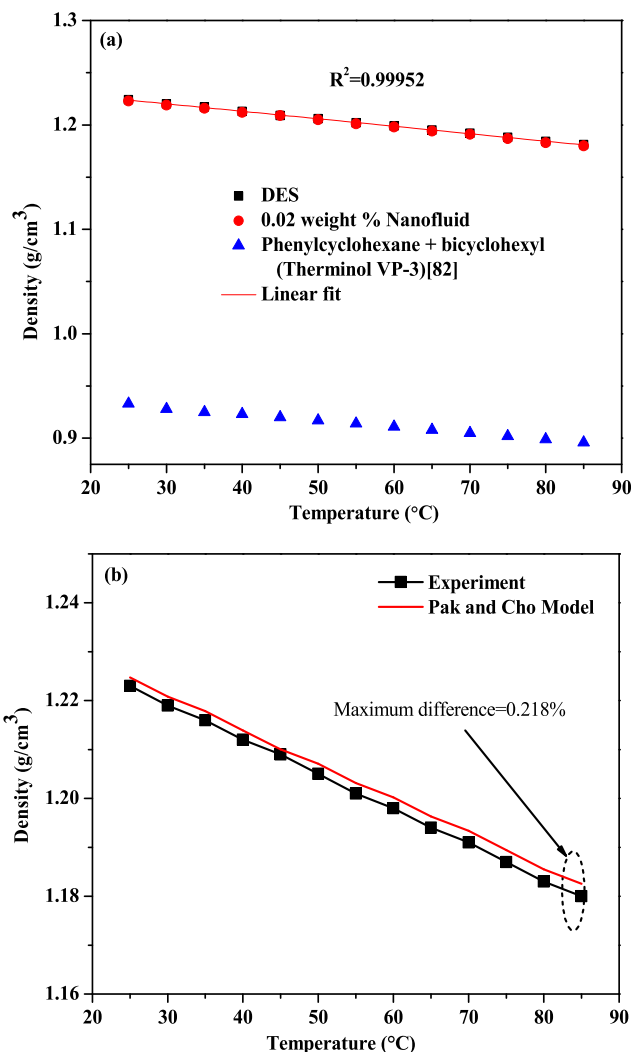
Fig. 10. (a) Variation of density with different temperatures for DES and nanofluids (b) Comparison plot of density between experimental with Pak and Cho Model [83].

movement of the molecule ensures that the rate of collision of molecules decreases. As a result, the thermal conductivity of DES decreases with increasing temperature.

The experimental measured values are correlated with the theoretical model as provided by Maxwell [89] and given in equation (8) (Fig. 13(b)). However this model does not give accurate thermal conductivity as it does not consider degree of aggregation, nanoparticle structure and Brownian motion [90]. A similar difference can be found in literature for other nanofluids [28,91].

$$k_{nf} = k_{bf} \left[\frac{k_{np} + 2k_{bf} + 2\varphi \left(k_{np} - k_{bf} \right)}{k_{np} + 2k_{bf} - \varphi \left(k_{np} - k_{bf} \right)} \right] \qquad (8)$$

Where, k_{nf}, k_{bf}, k_{np} and φ are thermal conductivity of nanofluid, basefluid, nanoparticle and volume fraction of the nanofluid respectively.

Fig. 14(a) shows the specific heat of DES and nanofluid at different temperatures from 45 °C to 90 °C with a heating rate 20 °C/min. It is clear from the data that specific heat increases with an increase in temperatures. However, the addition of multi-walled carbon nanotube enhances the heat capacity of the nanofluid. Furthermore, the specific heat capacity of both nanofluid and base fluid is higher than *Therminol VP-3*. Further, it was reported that the specific heat of nanofluid decreases with increasing particle volume concentrations [92]. This can be attributed to the fact that
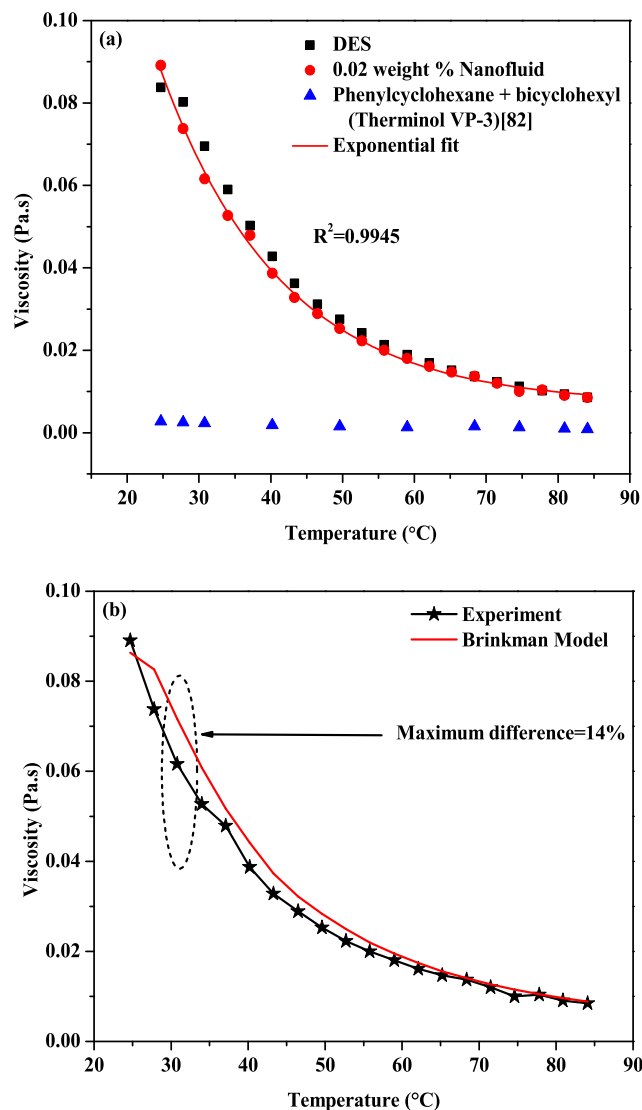

Fig. 11. (a) Variations of viscosity at different temperatures for DES and nanofluids (b) Comparison plot of viscosity between experimental and Brinkman model [84].
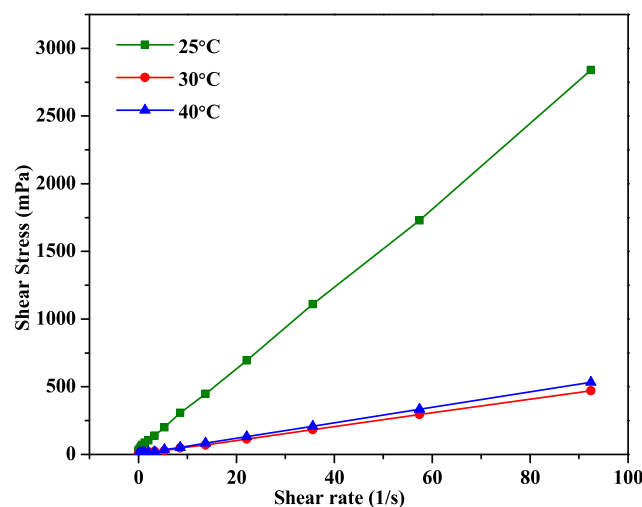

Fig. 12. Shear stress versus shear rate of nanofluid at three different temperatures.
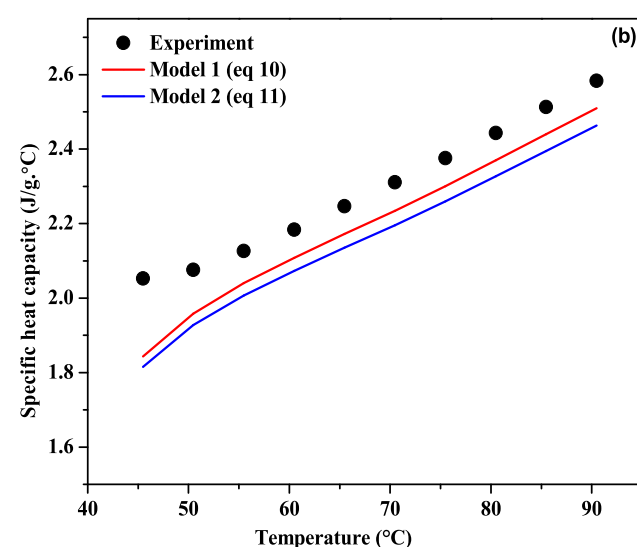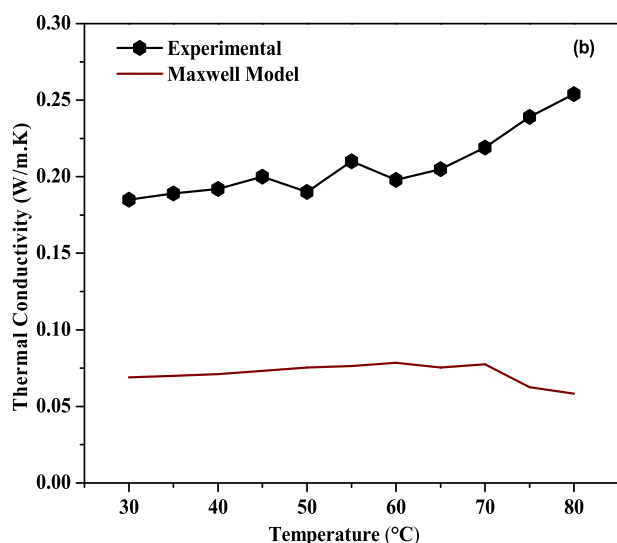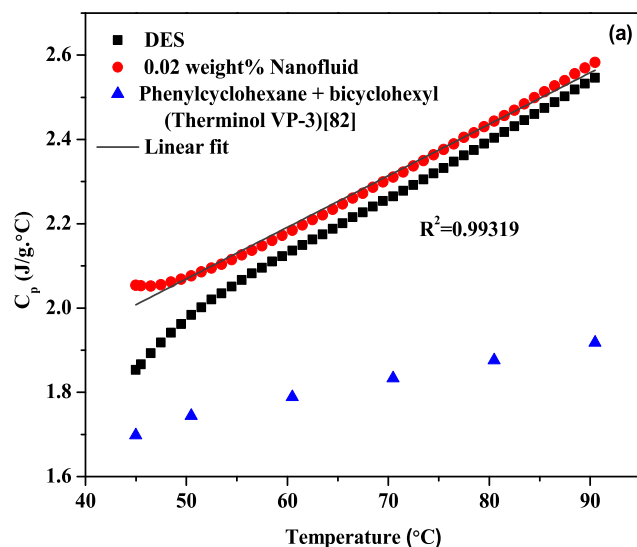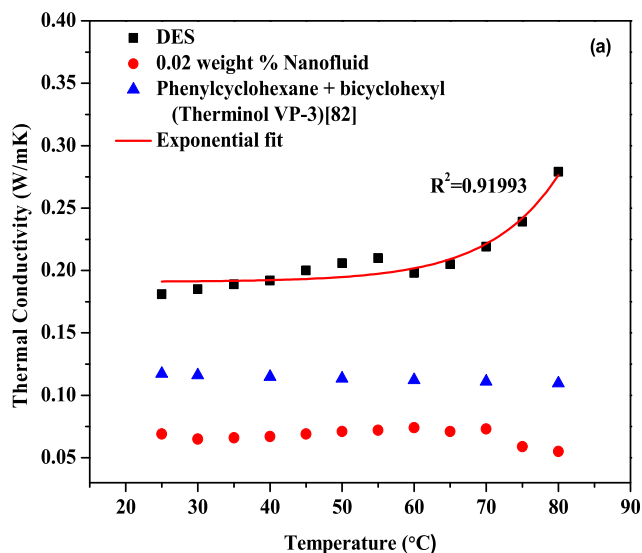
Fig. 13. (a) Variation of thermal conductivity at different temperatures for DES and nanofluids (b) Comparison plot of thermal conductivity between experimental and Maxwell model [89].

Fig. 14. (a) Variation of specific heat at different temperatures for DES and nanofluids (b) Comparison plot of specific heat between experimental data and theoretical models [28].

to increase the temperature, the internal energy increases, which implies a rise in vibrational energy and rotational energy of the molecules. This in turn, allows the molecule to adsorb high molar heat capacity. Based on the experimental data with the function of temperature, a mathematical correlation was developed as shown in Fig. 14(a) and given below:.

$$Cp = 0.01223T + 1.45749 \tag{9}$$

Here Cp and is T are the specific heat capacity and temperature of the nanofluid..

There are two widely used theoretical models which correlate the experimental data are based on the straight average of specific heat capacities (equation (10)) and thermal equilibrium between particle-liquid (equation (11))[28].

$$Model1 : Cp_{nf} = \varphi_v Cp_{np} + (1 - \varphi_v)Cp_{bf} \tag{10}$$

$$Model2 : Cp_{nf} = \frac{\varphi_v Cp_{np}\rho_{np} + (1 - \varphi_v)Cp_{bf}\rho_{bf}}{\varphi_v \rho_{np} + (1 - \varphi_v)\rho_{bf}} \tag{11}$$

Here Cp_{nf}, Cp_{np}, Cp_{bf} are the specific heat of the nanofluid, nanoparticle, and base fluid, respectively. ρ_{np}, ρ_{np}, ρ_{bf} are the density of nanofluid, nanoparticle, and base fluid, respectively. φ_v is the volume fraction. A comparison between theoretical models and experimental measured values is shown in Fig. 14(b). Significance difference was observed from the experimental values to the theoretical models. Possible reasons that are reported in the literature and are not considered in these models are nanoparticle size, shape, and degree of aggregation [93].

We have found comparable results of thermal conductivity value with Ilyas et al.[28]. The values of thermal conductivity were directly proportional to the temperature. In our work, 184.61% and 65.10% enhancement was observed at temperatures 30 °C and 40 °C, whereas a maximum enhancement 28.7% was observed by Ilyas et al.[28]. Additionally, we compared our results to published literature [93–96] and found that, in both circumstances, the specific heat value rises as the temperature rises.

4.6. MD simulations

The thermal conductivity is usually computed through the equation (12).

$$J = -\lambda \nabla T \tag{12}$$

Where, ∇T is the gradient of the temperature T, J is the resulting heat flux vector. Microscopically thermal conductivity can be defined in terms of time average is.

$$\lambda = \lim_{\partial t/\partial z \to 0} \lim_{t \to \infty} -\frac{\langle J_z(t) \rangle}{\langle \frac{\partial t}{\partial z} \rangle} \tag{13}$$

Here we are interested in isotropic fluids with collinear temperature gradients and heat fluxes, and thermal conductivity is considered to be scalar. The natural simulation experiment, similar to actual experimental observations, would be to impose a temperature gradient on the simulated system, compute the heat flow parallel to the gradient, and use equation (1) to derive the thermal conductivity. However, since heat flux is a highly fluctuating quantity, its average converges slowly, necessitating the use of substantial temperature gradients to create a heat flow identifiable from noise. As a result, we go in the other way. We apply a heat flux to the system and record the temperature gradient that results. This has the benefit of ensuring that the slowly convergent amount of heat flow is known precisely and does not need calculation. On the other hand, the temperature and its gradient are averages derived over time and over a large number of particles, making them more defined and fast convergent.

The simulation box is split into N slabs perpendicular to the z direction in order to impose a heat flow and compute a temperature profile. The slabs in this piece are selected to be similar in thickness and hence volume. The instantaneous local kinetic temperature T_K in slab k is defined as.

$$T_K = \frac{1}{3n_k k_B} \sum_{i \in k}^{n_k} m_i v_i^2 \tag{14}$$

Where, the sum extends over the n_k atoms i in slab k with masses m_i, k_B is the Boltzmann constant. Here the Initial slab is designated as the lowest temperature slab, while slab in the midpoint is designated as the hotter slab. The heat flux is created by exchanging the velocity vectors of an atom in the cool slab and one in the hot slab in such a manner that the temperature in the hot slab rises and the temperature in the cool slab lowers. Due to the large variation of atomic kinetic energies in comparison to the temperature difference between the two slabs, the hottest atom in the cool slab had greater kinetic energy than the coldest atom in the hot slab. This results in a transfer of energy from the cool slab to the heated slab and a temperature gradient between the cold and hot slabs. Thus by exchanging the velocities of two particles of equal helps it in maintaining the total linear momentum, total kinetic energy, and total energy in a conservative system. Here the velocity exchange is fulfils all the conservation principles.

After attaining steady state, the energy transfer forced by the unphysical velocity exchange is precisely balanced by the heat flow in the opposite direction caused by the system's thermal conductivity. On the other hand, the imposed heat flux is known precisely, since it is calculated by adding the "quanta" of energy carried by velocity exchanges. The temperature gradient that persists in steady state is exactly proportional to the thermal conductivity. Thermal conductivity is calculated as.

$$\lambda = -\frac{\sum_{transfers} \frac{m}{2}(v_h^2 - v_c^2)}{2tL_xL_y \langle \partial t/\partial z \rangle} \tag{15}$$
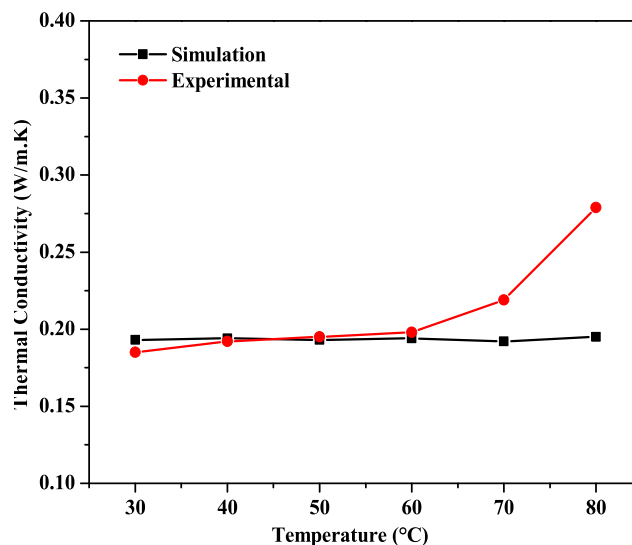

Fig. 15. Comparison of experimental and MD predicted thermal conductivity values.

The sum is taken over all transfer events during the simulation time t. The subscript h and c refer to the hot and cold particle of identical mass m whose velocities are interchanged. L_x and L_y represent the box length in x and y direction. Factor 2 in denominator represent the periodicity of the arrangement.

Thermal conductivity values of nanofluid calculated at 30, 40, 50, 60, 70, and 80 °C. The values of thermal conductivities obtained were 0.1937(30 °C), 0.1944(40 °C), 0.1935(50 °C), 0.1937(60 °C), 0.1905(70 °C), and 0.1922(80 °C). The experimental values obtained at different temperatures are also shown in Fig. 15. The values of thermal conductivity at 40 °C is found to be a good match with the experiment. However, the simulations failed to reproduce the experimental trend from 30 to 40 °C. A Major deviation was observed when compared with experimental values from 60 °C. The particle–fluid interface may have attributed this deviation, whereas this interaction is not considered in the simulation. The results from the mentioned manuscript showed that even though the experimental values change with temperature, the simulated values show minimal change.

5. Conclusion

This current work aims to characterize the MWCNT nanoparticle and synthesized MWCNT based nanofluid by a two-step method of preparation. The nanofluid was prepared by mixing DES (MTPB salt and ethylene glycol in the molar ratio of 1:4) and 0.02 wt% of MWCNT. Thereafter the thermophysical properties, including thermal conductivity, viscosity, density, and specific heat of the nanofluid, were measured. MWCNT was characterized by FETEM and FESEM to visualize the morphology of the nanoparticles. Further from FT-IR and powder XRD experiment, conjugation of DES attached with MWCNT and crystallinity of the MWCNT was confirmed. Stability of the nanofluid was investigated through visual observation, optical microscope as well as zeta potential. The density and viscosity was found to decrease with an increase in the nanofluid temperature when 0.02 wt% MWCNT is added. The DES exhibits Newtonian behavior, as evidenced by the fact that its shear viscosity decreases with increasing temperature. At higher temperatures, there is a significant increase in thermal conductivity and specific heat. The thermophysical properties of nanofluid qualities revealed that it outperforms the traditional

commercial HTFs and that it has tremendous promise for use as an advanced Heat Transfer Fluid in Concentrated Solar Power (CSP) and Multi-Stage Flash (MSF) column plants.

CRediT authorship contribution statement

Nipu Kumar Das: Conceptualization, Methodology, Software, Investigation, Resources, Writing – original draft. **Papu Kumar Naik:** Validation, Formal analysis, Data curation, Visualization. **Dhileep N. Reddy:** MD Methodology. **Bhabani S. Mallik:** MD Methodology. **Surya Sarathi Bose: Tamal Banerjee:** Writing – review & editing, Supervision.

Declaration of Competing Interest

The authors declare that they have no known competing financial interests or personal relationships that could have appeared to influence the work reported in this paper.

Acknowledgments

References

[1] N. Menges, The role of green solvents and catalysts at the future of drug design and of synthesis, Green Chem. 23 (2017) 254–257.

[2] E. Durand, J. Lecomte, B. Baréa, G. Piombo, E. Dubreucq, P. Villeneuve, Evaluation of deep eutectic solvents as new media for Candida antarctica B lipase catalyzed reactions, Process. Biochem. 47 (12) (2012) 2081–2089.

[3] A.E. Ünlü, A. Arıkaya, S. Takaç, Use of deep eutectic solvents as catalyst: A mini-review, Green Process. Synth, 8 (1) (2019) 355–372.

[4] E.L. Smith, A.P. Abbott, K.S. Ryder, Deep eutectic solvents (DESs) and their applications, Chem. Rev. 114 (21) (2014) 11060–11082.

[5] Y. Liu, J.B. Friesen, J.B. McAlpine, D.C. Lankin, S.-N. Chen, G.F. Pauli, Natural deep eutectic solvents: properties, applications, and perspectives, J. Nat. Prod. 81 (3) (2018) 679–690.

[6] R.D. Rogers, K.R. Seddon, S. Volkov, Green industrial applications of ionic liquids. Vol. 92. 2012: Springer Science & Business Media.

[7] N.R. Varma, A. Ramalingam, T. Banerjee, Experiments, correlations and COSMO-RS predictions for the extraction of benzothiophene from n-hexane using imidazolium-based ionic liquids, Chem. Eng. J. 166 (1) (2011) 30–39.

[8] L. Kumar, T. Banerjee, K. Mohanty, Prediction of selective extraction of cresols from aqueous solutions by ionic liquids using theoretical approach, Sep. Sci. Technol. 46 (13) (2011) 2075–2087.

[9] A.A.P. Kumar, T. Banerjee, Thiophene separation with ionic liquids for desulphurization: A quantum chemical approach, Fluid Phase Equilib. 278 (1–2) (2009) 1–8.

[10] S.R. Pilli, T. Banerjee, K. Mohanty, Ionic liquids as green solvents for the extraction of endosulfan from aqueous solution: a quantum chemical approach, Chem. Prod. Process Model. 8 (1) (2013) 1–14.

[11] D. Rabari, T. Banerjee, Experimental and theoretical studies on the effectiveness of phosphonium-based ionic liquids for butanol removal at T= 298.15 K and p= 1 atm, Ind. Eng. Chem. Res. 53 (49) (2014) 18935–18942.

[12] A. Nann, C. Held, G. Sadowski, Liquid–liquid equilibria of 1-butanol/water/IL systems, Ind. Eng. Chem. Res. 52 (51) (2013) 18472–18481.

[13] D. Rabari, T. Banerjee, Biobutanol and n-propanol recovery using a low density phosphonium based ionic liquid at T= 298.15 K and p= 1 atm, Fluid Phase Equilib. 355 (2013) 26–33.

[14] B. Wu, R.G. Reddy, R.D. Rogers, Novel ionic liquid thermal storage for solar thermal electric power systems, in: International Solar Energy Conference, 2001: American Society of Mechanical Engineers.

[15] K. Jafari, M.H. Fatemi, P. Estellé, Deep eutectic solvents (DESs): A short overview of the thermophysical properties and current use as base fluid for heat transfer nanofluids, J. Mol. Liq. 321 (2021) 114752.

[16] C. Liu, H. Fang, X. Liu, B. Xu, Z. Rao, Novel silica filled deep eutectic solvent based nanofluids for energy transportation, ACS Sustainable Chem. Eng. 7 (24) (2019) 20159–20169.

[17] Y.u. Chen, T. Mu, Application of deep eutectic solvents in biomass pretreatment and conversion, Green Energy Environ. 4 (2) (2019) 95–115.

[18] A. Shishov, A. Bulatov, M. Locatelli, S. Carradori, V. Andruch, Application of deep eutectic solvents in analytical chemistry, A review, Microchemical Journal 135 (2017) 33–38.

[19] S.U. Choi and J.A. Eastman, Enhancing thermal conductivity of fluids with nanoparticles. 1995, Argonne National Lab.(ANL), Argonne, IL (United States).

[20] A. Karimipour, S.A. Bagherzadeh, M. Goodarzi, A.A. Alnaqi, M. Bahiraei, M.R. Safaei, M.S. Shadloo, Synthesized CuFe2O4/SiO2 nanocomposites added to water/EG: evaluation of the thermophysical properties beside sensitivity analysis & EANN, Int. J. Heat Mass Transf. 127 (2018) 1169–1179.

[21] A. Ghasemi, M. Hassani, M. Goodarzi, M. Afrand, S. Manafi, Appraising influence of COOH-MWCNTs on thermal conductivity of antifreeze using curve fitting and neural network, Physica A 514 (2019) 36–45.

[22] S.A. Bagherzadeh, A. D'Orazio, A. Karimipour, M. Goodarzi, Q.-V. Bach, A novel sensitivity analysis model of EANN for F-MWCNTs–Fe3O4/EG nanofluid thermal conductivity: Outputs predicted analytically instead of numerically to more accuracy and less costs, Physica A 521 (2019) 406–415.

[23] R.E. Smalley, Carbon nanotubes: synthesis, structure, properties, and applications (2003).

[24] A. Asadi, I.M. Alarifi, V. Ali, H.M. Nguyen, An experimental investigation on the effects of ultrasonication time on stability and thermal conductivity of MWCNT-water nanofluid: Finding the optimum ultrasonication time, Ultrason. Sonochem. 58 (2019) 104639, https://doi.org/10.1016/j.ultsonch.2019.104639.

[25] I. Mahbubul, R. Saidur, M. Amalina, M. Niza, Influence of ultrasonication duration on rheological properties of nanofluid: an experimental study with alumina–water nanofluid, Int. Commun. Heat Mass Transfer 76 (2016) 33–40.

[26] Y. Hwang, J.K. Lee, C.H. Lee, Y.M. Jung, S.I. Cheong, C.G. Lee, B.C. Ku, S.P. Jang, Stability and thermal conductivity characteristics of nanofluids, Thermochim Acta 455 (1-2) (2007) 70–74.

[27] A.O. Borode, N.A. Ahmed, P.A. Olubambi, A review of heat transfer application of carbon-based nanofluid in heat exchangers, Nano-Structures & Nano-Objects 20 (2019) 100394.

[28] S.U. Ilyas, R. Pendyala, M. Narahari, Stability and thermal analysis of MWCNT-thermal oil-based nanofluids, Colloids Surf., A 527 (2017) 11–22.

[29] M.A. Salam, R. Burk, Synthesis and characterization of multi-walled carbon nanotubes modified with octadecylamine and polyethylene glycol, Arabian J. Chem. 10 (2017) S921–S927.

[30] W. Yu, H. Xie, A review on nanofluids: preparation, stability mechanisms, and applications, Journal of nanomaterials 2012 (2012).

[31] K.V. Wong and O. De Leon, Applications of nanofluids: current and future, in Nanotechnology and Energy. 2017, Jenny Stanford Publishing. p. 105-132.

[32] H.B. Ma, C. Wilson, B. Borgmeyer, K. Park, Q. Yu, S.U.S. Choi, M. Tirumala, Effect of nanofluid on the heat transport capability in an oscillating heat pipe, Appl. Phys. Lett. 88 (14) (2006) 143116, https://doi.org/10.1063/1.2192971.

[33] H. Ma, C. Wilson, Q. Yu, K. Park, U. Choi, and M. Tirumala, An experimental investigation of heat transport capability in a nanofluid oscillating heat pipe, (2006).

[34] P.X. Tran, D. Lyons, Nanofluids for use as ultra-deep drilling fluids, Fact Sheet, National Energy Technology Laboratory, Office of Fossil Energy, US Department of Energy, Jan, netl. doe. gov/publications/factsheets/rd/R&D108 (2007) pdf. http://www.

[35] S. Vafaei, T. Borca-Tasciuc, M.Z. Podowski, A. Purkayastha, G. Ramanath, P.M. Ajayan, Effect of nanoparticles on sessile droplet contact angle, Nanotechnology 17 (10) (2006) 2523–2527.

[36] W. Chen, C. Zou, X. Li, H. Liang, Application of recoverable carbon nanotube nanofluids in solar desalination system: An experimental investigation, Desalination 451 (2019) 92–101.

[37] R.S. Shawgo, A.C. Richards Grayson, Y. Li, M.J. Cima, BioMEMS for drug delivery, Curr. Opin. Solid State Mater. Sci. 6 (4) (2002) 329–334.

[38] A. Ovsianikov, B. Chichkov, P. Mente, N.A. Monteiro-Riviere, A. Doraiswamy, R.J. Narayan, Two photon polymerization of polymer–ceramic hybrid materials for transdermal drug delivery, Int. J. Appl. Ceram. Technol. 4 (1) (2007) 22–29.

[39] J.-F. Yan, J. Liu, Nanocryosurgery and its mechanisms for enhancing freezing efficiency of tumor tissues, Nanomedicine: Nanotechnology, Biology and Medicine 4 (1) (2008) 79–87.

[40] P.-C. Chiang, D.-S. Hung, J.-W. Wang, C.-S. Ho, Y.-D. Yao, Engineering water-dispersible FePt nanoparticles for biomedical applications, IEEE Trans. Magn. 43 (6) (2007) 2445–2447.

[41] B. Chitra, K.S. Kumar, Heat transfer enhancement using single base and double base nanofluids, J. Mol. Liq. 221 (2016) 1128–1132.

[42] J.A. Eastman, S.U.S. Choi, S. Li, W. Yu, L.J. Thompson, Anomalously increased effective thermal conductivities of ethylene glycol-based nanofluids containing copper nanoparticles, Appl. Phys. Lett 78 (6) (2001) 718–720.

[43] S.M.S. Murshed, K.C. Leong, C. Yang, Enhanced thermal conductivity of TiO2—water based nanofluids, Int. J. Therm. Sci. 44 (4) (2005) 367–373.

[44] Y. Xuan, Q. Li, Heat transfer enhancement of nanofluids, Int. J. Heat Fluid Flow 21 (1) (2000) 58–64.

[45] Y. Hwang, J.-K. Lee, J.-K. Lee, Y.-M. Jeong, S.-i. Cheong, Y.-C. Ahn, S.H. Kim, Production and dispersion stability of nanoparticles in nanofluids, Powder Technol. 186 (2) (2008) 145–153.

[46] E.K. Goharshadi, S. Samiee, P. Nancarrow, Fabrication of cerium oxide nanoparticles: Characterization and optical properties, J. Colloid Interface Sci. 356 (2) (2011) 473–480.

[47] E.K. Goharshadi, S.H. Sajjadi, R. Mehrkhah, P. Nancarrow, Sonochemical synthesis and measurement of optical properties of zinc sulfide quantum dots, Chem. Eng. J. 209 (2012) 113–117.

[48] H.-T. Zhu, Y.-S. Lin, Y.-S. Yin, A novel one-step chemical method for preparation of copper nanofluids, J. Colloid Interface Sci. 277 (1) (2004) 100–103.

[49] M.A. Khairul, K. Shah, E. Doroodchi, R. Azizian, B. Moghtaderi, Effects of surfactant on stability and thermo-physical properties of metal oxide nanofluids, Int. J. Heat Mass Transf. 98 (2016) 778–787.

[50] L. Yang, K. Du, X.S. Zhang, B.o. Cheng, Preparation and stability of Al2O3 nano-particle suspension of ammonia–water solution, Appl. Therm. Eng. 31 (17-18) (2011) 3643–3647.

[51] M. Mehrali, E. Sadeghinezhad, S.T. Latibari, S.N. Kazi, M. Mehrali, M.N.B.M. Zubir, H.S.C. Metselaar, Investigation of thermal conductivity and rheological properties of nanofluids containing graphene nanoplatelets, Nanoscale Res. Lett. 9 (1) (2014) 1–12.

[52] L. Vandsburger, Synthesis and covalent surface modification of carbon nanotubes for preparation of stabilized nanofluid suspensions, (2009).

[53] P. Dehury, J. Singh, T. Banerjee, Thermophysical and Forced Convection Studies on (Alumina+ Menthol)-Based Deep Eutectic Solvents for Their Use as a Heat Transfer Fluid, ACS Omega 3 (12) (2018) 18016–18027.

[54] D. Van Der Spoel, E. Lindahl, B. Hess, G. Groenhof, A.E. Mark, H.J. Berendsen, GROMACS: fast, flexible, and free, J. Comput. Chem. 26 (16) (2005) 1701–1718.

[55] M.J. Abraham, T. Murtola, R. Schulz, S. Páll, J.C. Smith, B. Hess, E. Lindahl, GROMACS: High performance molecular simulations through multi-level parallelism from laptops to supercomputers, SoftwareX 1 (2015) 19–25.

[56] S. Plimpton, Fast parallel algorithms for short-range molecular dynamics, J. Comput. Phys. 117 (1) (1995) 1–19.

[57] W.L. Jorgensen, D.S. Maxwell, J. Tirado-Rives, Development and testing of the OPLS all-atom force field on conformational energetics and properties of organic liquids, J. Am. Chem. Soc. 118 (45) (1996) 11225–11236.

[58] H. Liu, E. Maginn, A molecular dynamics investigation of the structural and dynamic properties of the ionic liquid 1-n-butyl-3-methylimidazolium bis (trifluoromethanesulfonyl) imide, J. Chem. Phys. 135 (12) (2011) 124507, https://doi.org/10.1063/1.3643124.

[59] N. Sieffert, G. Wipff, The [BMI][Tf2N] ionic liquid/water binary system: A molecular dynamics study of phase separation and of the liquid− liquid interface, J. Phys. Chem. B 110 (26) (2006) 13076–13085.

[60] T.D.N. Reddy, B.S. Mallik, Protic ammonium carboxylate ionic liquids: insight into structure, dynamics and thermophysical properties by alkyl group functionalization, PCCP 19 (16) (2017) 10358–10370.

[61] W. Humphrey, A. Dalke, K. Schulten, VMD: Visual molecular dynamics, J. Mol. Graph. 14 (1) (1996) 33–38, https://doi.org/10.1016/0263-7855(96)00018-5.

[62] M. Frisch and F. Clemente, Gaussian 09, Revision A. 01, MJ Frisch, GW Trucks, HB Schlegel, GE Scuseria, MA Robb, JR Cheeseman, G, Scalmani, V. Barone, B. Mennucci, GA Petersson, H. Nakatsuji, M. Caricato, X. Li, HP Hratchian, AF Izmaylov, J, Bloino, G. Zhe (2009).

[63] A.D. Becke, Density-functional exchange-energy approximation with correct asymptotic behavior, Phys. Rev. A 38 (6) (1988) 3098–3100.

[64] A. Becke, Density-functional thermochemistry. III. The role of exact exchange (1993) J, Chem. Phys 98 5648.

[65] C. Lee, W. Yang, R.G. Parr, Development of the Colle-Salvetti correlation-energy formula into a functional of the electron density, Physical review B 37 (2) (1988) 785–789.

[66] J. Wang, W. Wang, P.A. Kollman, D.A. Case, Automatic atom type and bond type perception in molecular mechanical calculations, J. Mol. Graph. Model. 25 (2) (2006) 247–260.

[67] L. Martínez, R. Andrade, E.G. Birgin, J.M. Martínez, PACKMOL: a package for building initial configurations for molecular dynamics simulations, J. Comput. Chem. 30 (13) (2009) 2157–2164.

[68] M.C. Payne, M.P. Teter, D.C. Allan, T. Arias, and a.J. Joannopoulos, Iterative minimization techniques for ab initio total-energy calculations: molecular dynamics and conjugate gradients, Reviews of modern physics 64(4) (1992) 1045.

[69] G. Bussi, D. Donadio, M. Parrinello, Canonical sampling through velocity rescaling, J. Chem. Phys. 126 (1) (2007) 014101, https://doi.org/10.1063/1.2408420.

[70] H.J.C. Berendsen, J.P.M. Postma, W.F. van Gunsteren, A. DiNola, J.R. Haak, Molecular dynamics with coupling to an external bath, J. Chem. Phys. 81 (8) (1984) 3684–3690.

[71] M. Parrinello, A. Rahman, Polymorphic transitions in single crystals: A new molecular dynamics method, J. Appl. Phys. 52 (12) (1981) 7182–7190.

[72] F. Müller-Plathe, A simple nonequilibrium molecular dynamics method for calculating the thermal conductivity, J. Chem. Phys. 106 (14) (1997) 6082–6085.

[73] M. Zhang, E. Lussetti, L.E.S. de Souza, F. Müller-Plathe, Thermal conductivities of molecular liquids by reverse nonequilibrium molecular dynamics, J. Phys. Chem. B 109 (31) (2005) 15060–15067.

[74] M.S. Kelkar, E.J. Maginn, Calculating the enthalpy of vaporization for ionic liquid clusters, J. Phys. Chem. B 111 (32) (2007) 9424–9427.

[75] C.M. Tenney, E.J. Maginn, Limitations and recommendations for the calculation of shear viscosity using reverse nonequilibrium molecular dynamics, J. Chem. Phys. 132 (1) (2010) 014103, https://doi.org/10.1063/1.3276454.

[76] H. Liu, E. Maginn, A.E. Visser, N.J. Bridges, E.B. Fox, Thermal and transport properties of six ionic liquids: an experimental and molecular dynamics study, Ind. Eng. Chem. Res. 51 (21) (2012) 7242–7254.

[77] P.K. Naik, S. Paul, T. Banerjee, Physiochemical properties and molecular dynamics simulations of phosphonium and ammonium based deep eutectic solvents, J. Solution Chem. 48 (7) (2019) 1046–1065.

[78] S.U. Ilyas, R. Pendyala, M. Narahari, L. Susin, Stability, rheology and thermal analysis of functionalized alumina-thermal oil-based nanofluids for advanced cooling systems, Energy Convers. Manage. 142 (2017) 215–229.

[79] W.U. Rehman, Z.M.A. Merican, A.H. Bhat, B.G. Hoe, A.A. Sulaimon, O. Akbarzadeh, M.S. Khan, A. Mukhtar, S. Saqib, A. Hameed, Synthesis, characterization, stability and thermal conductivity of multi-walled carbon nanotubes (MWCNTs) and eco-friendly jatropha seed oil based nanofluid: An experimental investigation and modeling approach, J. Mol. Liq. 293 (2019) 111534.

[80] P. Vadasz, Heat conduction in nanofluid suspensions, (2006).

[81] D. Lee, J.-W. Kim, B.G. Kim, A new parameter to control heat transport in nanofluids: surface charge state of the particle in suspension, J. Phys. Chem. B 110 (9) (2006) 4323–4328.

[82] Therminol_VP3 heat transfer fluid; Available from: https://www.therminol.com/sites/therminol/files/documents/TF22A_Therminol_VP3.pdf.

[83] B.C. Pak, Y.I. Cho, Hydrodynamic and heat transfer study of dispersed fluids with submicron metallic oxide particles, Exp. Heat Transf. 11 (2) (1998) 151–170.

[84] O. Mahian, A. Kianifar, C. Kleinstreuer, M.A. Al-Nimr, I. Pop, A.Z. Sahin, S. Wongwises, A review of entropy generation in nanofluid flow, Int. J. Heat Mass Transf. 65 (2013) 514–532.

[85] S.U. Ilyas, R. Pendyala, N. Marneni, Preparation, sedimentation, and agglomeration of nanofluids, Chem. Eng. Technol. 37 (12) (2014) 2011–2021.

[86] A. Beheshti, M. Shanbedi, S.Z. Heris, Heat transfer and rheological properties of transformer oil-oxidized MWCNT nanofluid, J. Therm. Anal. Calorim. 118 (3) (2014) 1451–1460.

[87] S. Dong, X. Chen, An improved model for thermal conductivity of nanofluids with effects of particle size and Brownian motion, J. Therm. Anal. Calorim. 129 (2) (2017) 1255–1263.

[88] S. Pil Jang and S.U. Choi, Effects of various parameters on nanofluid thermal conductivity, (2007).

[89] M.G. Jc, Colours in metal glasses and in metallic films, Philos. Trans. Roy. Soc. London 203 (1904) 385–420.

[90] P. Keblinski, S.R. Phillpot, S.U.S. Choi, J.A. Eastman, Mechanisms of heat flow in suspensions of nano-sized particles (nanofluids), Int. J. Heat Mass Transf. 45 (4) (2002) 855–863.

[91] X. Li, C. Zou, Lu. Zhou, A. Qi, Experimental study on the thermo-physical properties of diathermic oil based SiC nanofluids for high temperature applications, Int. J. Heat Mass Transf. 97 (2016) 631–637.

[92] S. Akilu, A. Baheta, K. Sharma, and M. Said. Experimental determination of nanofluid specific heat with SiO2 nanoparticles in different base fluids, in AIP Conference Proceedings, 2017: AIP Publishing LLC.

[93] B.-X. Wang, L.-P. Zhou, X.-F. Peng, Surface and size effects on the specific heat capacity of nanoparticles, Int. J. Thermophys. 27 (1) (2006) 139–151.

[94] M. Saeedian, M. Mahjour-Shafiei, E. Shojaee, M.R. Mohammadizadeh, Specific heat capacity of TiO2 nanoparticles, J. Comput. Theor. Nanosci. 9 (4) (2012) 616–620.

[95] P. Andreu-Cabedo, R. Mondragon, L. Hernandez, R. Martinez-Cuenca, L. Cabedo, J.E. Julia, Increment of specific heat capacity of solar salt with SiO 2 nanoparticles, Nanoscale Res. Lett. 9 (1) (2014) 1–11.

[96] S.M.M. Rizvi, D. Shin, Specific heat capacity, viscosity, and thermal stability of carbonate-based molten salt nanofluids, J. Storage Mater. 43 (2021) 103192.